Single Red Blood Cell Oxygenation Saturation Imaging with Multispectral Photoacoustic Microscopy

Michael J. Moore*†, Patrick M. Schygulla*‡, Eric M. Strohm*†, and Michael C. Kolios*†
* Department of Physics, Ryerson University, Toronto, Ontario, Canada
† Institute for Biomedical Engineering and Science Technology , Toronto, Ontario, Canada
‡Department of Physics and Astronomy, Heidelberg University, Heidelberg, Germany

***Abstract*—In the last decade, photoacoustic techniques have been used extensively to acquire label free oxygen saturation (SO_2) images of blood vessels both *in vivo* and *ex vivo*. Recent advances in photoacoustic microscopy have pushed the *in vivo* resolution limit of photoacoustic SO_2 mapping to that of a single cell. In this work, we use a photoacoustic microscope equipped with a 0.9 GHz ultrasound transducer and a fiber coupled 532 nm Nd:YAG laser source to generate sub-cellular resolution SO_2 maps of single red blood cells (RBC) *ex vivo*. Stimulated Raman scattering (SRS) within the optical fiber produces secondary peaks in the laser output spectrum, which can be isolated as discrete photoacoustic excitation sources by using optical bandpass filters. Photoacoustic images acquired at the different excitation wavelengths are co-registered, and a local SO_2 map for the RBC is created. Untreated RBCs, as well as RBCs that had been chemically deoxygenated with sodium dithionite were imaged with the system. The resultant SO_2 maps show a high percentage of SO_2 through out the untreated cell, as well as localized pockets of both high and low SO_2 in the treated cell. For the untreated cell, the mean and median SO_2 values were 72 and 73%, respectively, while for the treated cell they were 56% and 57%. This multispectral PA technique has potential applications in assessing chromophore distribution and oxygen transfer kinetics at the sub-cellular level.**

I. Introduction

One of the primary functions of red blood cells (RBC) in humans is the transport of oxygen throughout the body [1]. Molecular oxygen reversibly binds to the heme group of the hemoglobin protein contained within the RBC cytosol and is deposited elsewhere in the body after traversing the vasculature. The binding of molecular oxygen to the heme group alters the structure of hemoglobin, causing a change in the absorption spectrum of the protein [2]. This change in absorption is readily detectable using optical techniques, for example: pulse oximetry [3], CO-oximetry [4], and fNIRS [5]. Furthermore, these techniques can be used to determine the oxygen saturation (SO_2) of the blood, i.e. the ratio of oxygenated hemoglobin (oxyhemoglobin) to total hemoglobin content (oxy- and deoxy-hemoglobin).

In the last decade, two photoacoustic (PA) techniques, photoacoustic tomography (PAT) and photoacoustic microscopy (PAM), have also been used for determining SO_2 values both *in vivo* and *ex vivo*. Zhang *et al*. used PAT to map the SO_2 in subcutaneous vessels of a Sprague-Dawley rat under normoxic and hypoxic conditions [6]. Around the same time, Wang *et al*. used PAT to non-invasively determine hemoglobin concentration as well as SO_2 in the Sprague-Dawley rat brain [7]. More recently, PAM has been used to acquire images of changes in the SO_2 and blood flow of vessels in the brain of a mouse as it responded to various stimuli [8]. In contrast to the previously mentioned techniques, which determine SO_2 at the capillary/vessel level, photoacoustic flowoxigraphy can be used to track the SO_2 change of individual RBCs *in vivo* [9]; however, using this technique, no detail within the RBC can be resolved.

Multispectral PAM setups typically employ tunable dye lasers [7], [10], or OPO lasers [11] to produce the wavelengths required for photoacoustic SO_2 assessment. However, through stimulated Raman scattering (SRS), monoenergetic lasers can also be used. In SRS, the photons from the laser source undergo inelastic collisions within the fiber, resulting in a Stoke's shift and the production of additional peaks in the laser spectrum at the fiber output [12]. The first use of this phenomenon in PAM was by Koeplinger *et al*., who generated PA images of tubes containing different coloured dyes, and could differentiate between them by the strength of the signal in the resultant PA images [13]. Hajireza *et al*. built a system that used SRS to generate wavelengths from 489 nm to 788 nm, and with a subset of those wavelengths acquired *in vivo* SO_2 maps of the capillary beds in a Swiss Webster mouse ear [14]. Recently, we used an ultra-high frequency PAM setup equipped with an SRS laser source to acquire high resolution images of individual leukocytes stained with Wright-Giemsa. Differentiation between various leukocyte subtypes was possible based on the unique features and signal strength in the PA images created [15], [16]. In this work, we use a similar setup to generate high-resolution PAM images of oxygenated and deoxygenated RBCs. Optical band-pass filters are used to select irradiation wavelengths about the 570 nm isosbestic point of oxy- and deoxy-hemoglobin, and an ultrasound transducer with a central frequency of 0.9 GHz is used to record emitted PA signals. The PA signals are then corrected for pulse-to-pulse variation in the incident laser energy, and used to create high resolution intracellular SO_2 maps.

978-1-4673-9897-8/16/$31.00 ©2016 IEEE

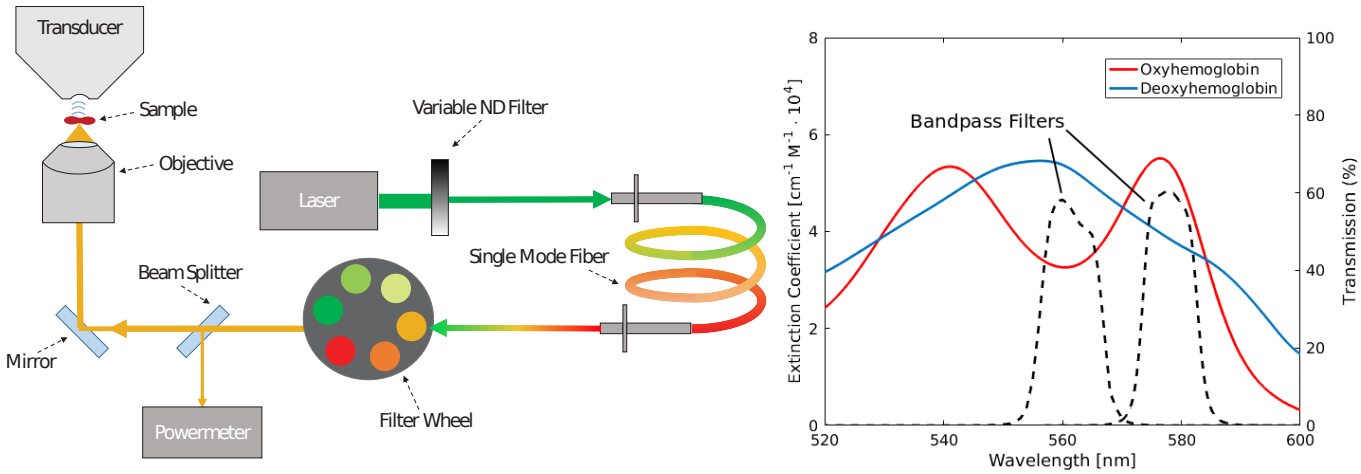

(a) (b)

Fig. 1. **a)** Schematic of the system setup. A pulsed 532 nm Nd:YAG laser is attenuated with a variable OD neutral density filter and coupled into a polarization maintaining single mode fiber. Stimulated Raman scattering within the fiber produced a spectrum of wavelengths. The wavelength used to irradiate the sample is then selected using a filter wheel. A portion of the beam is then redirected to a power meter for pulse-to-pulse energy monitoring. The transmitted beam is reflected off a dichroic mirror and focused using a 20X objective onto the sample. An ultrasound transducer with 0.9 GHz central frequency confocal with the microscope objective focus is used to record emitted PA waves. **b)** The red and blue solid lines show the extinction coefficient for oxy- and deoxy-hemoglobin, respectively. The dashed lines show the transmission characteristics for the two optical filters used for wavelength selection.

II. Methods

A. Sample Preparation

Human RBCs were extracted via finger prick from a healthy volunteer in accordance with Ryerson research ethics board protocol 2012-210-1, and immediately diluted in 50 µL of 1X PBS. To this, 150 µL of a 1% (v/v) glutaraldehyde solution in PBS was added to fix the cells. After 5 minutes, 100 µL of the fixed RBC solution was pipetted into a separate aliquot, to which 50 µL of 0.3% (w/v) sodium dithionite, a chemical commonly used to induce deoxygenated status in RBCs [17], in PBS was then added. Both oxygenated (untreated) and deoxygenated (treated) samples were then vortexed at 1800 rpm for 10 seconds. Two microliters of each sample were then added to separate Poly-D-Lysine coated glass bottom petri dishes (Mattek, USA) filled with 4 mL of PBS. The dishes were kept in a climate controlled environment at 37^{o}C prior to measurement.

B. System Setup

The photoacoustic system setup used in this experiment is shown in Figure 1a. A 532 nm Nd:YAG laser (Teem Photonics, France) operating at a 4 kHz pulse repetition frequency was used for all photoacoustic experiments. The laser energy at the input end of the fiber was controlled by translating a ND filter with continuously varying optical density (Thorlabs, USA) through the beam path using a micrometer. The SRS effect within the single-mode fiber (Coastal Connections, USA) produced peaks at 532 (pump), 545, 559 and 575 nm. The laser beam exiting the fiber was collimated and directed through a filter wheel, which was used to rotate an optical bandpass filter into the beam path. There were two filters used in this experiment: the first had a central wavelength of 560 nm, and the second had a central wavelength of 577 nm. Both filters had a spectral FWHM of 10 nm. The transmission spectra of the two bandpass filters are shown in Figure 1b along with the extinction coefficient spectrum for oxy- and deoxy-hemoglobin. After passing through the filter wheel, the laser beam was split; the transmitted portion of the beam entered the side port of the photoacoustic microscope (kibero GmbH, Germany), and the reflected portion was directed into a Mach6 energy meter (Gentec-EO, Canada) for pulse-to-pulse energy measurements. The transmitted beam was focused onto the sample using a 20X microscope objective with a NA of 0.4 (Olympus, Japan), aligned confocally with a 0.9 GHz central frequency ultrasound transducer on the opposite side of the sample.

C. Image Acquisition

The petri dish containing the untreated cells was placed on the microscope translation stage. RBCs in the dish were located using the microscope optics, translated into the confocal laser/ultrasound focus, and then scanned using a raster pattern. PA images were acquired first with the 560 nm bandpass filter, and immediately after with the 577 nm filter. The fast- and slow-scan step sizes were 0.15 µm, and total of 100 RF-lines were acquired at each scanning position. At each scan position, the individual RF-lines were normalized by the corresponding pulse energies read at the energy meter, and were then averaged to increase SNR. Maximum amplitude projection images at both wavelengths were formed using the respective normalized data sets. An identical procedure was followed for the treated RBCs.

D. SO_2 Calculation

The normalized images at both wavelengths were co-registered and pseudo-coloured. Images acquired at 560 nm

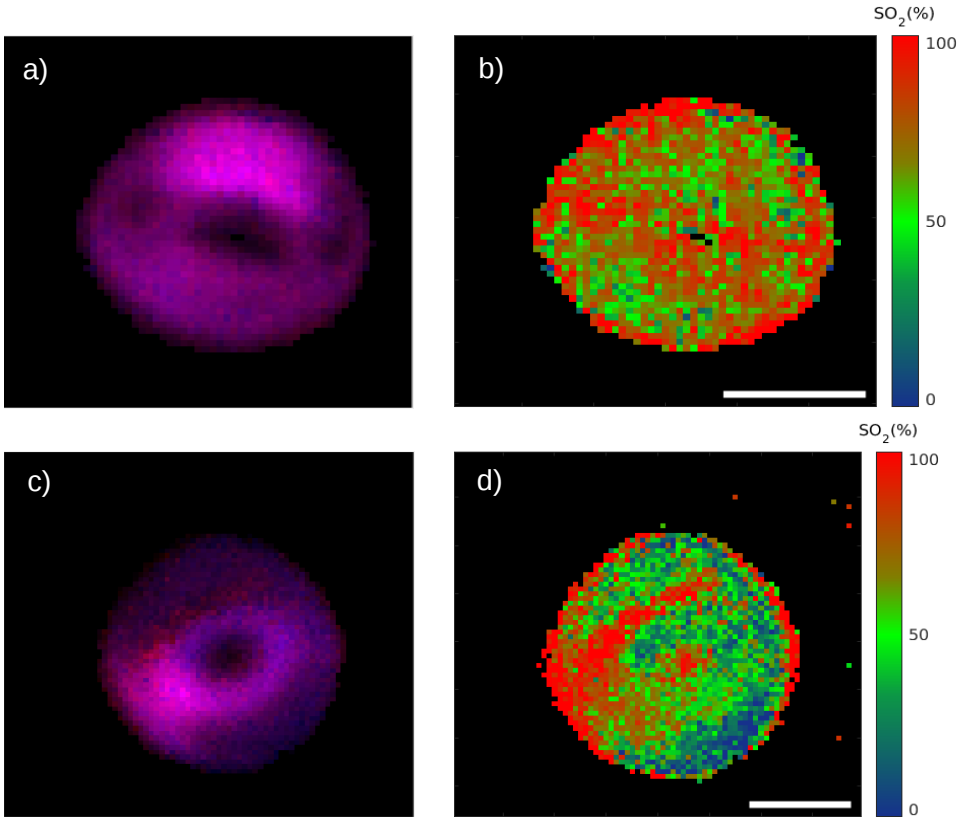

Fig. 2. **a)** Fused image of untreated RBC at 560 nm (blue channel) and 577 nm (red channel). **b)** SO_2 map of a) obtained using the MMSE algorithm. **c)** Fused image of sodium dithionite treated RBC at 560 nm (blue channel) and 577 nm (red channel). **d)** SO_2 map of c) using the MMSE algorithm. The scale bars are 3 µm.

were coloured blue, while images acquired at 577 nm were pseudo-coloured red. The resultant 560 and 577 nm images were then assigned to the blue and red channels of a fused RGB image, respectively. A constrained mean square error (MMSE) algorithm was used to calculate the percent SO_2 value at each pixel, following the method of Kim *et al.* [11]. The algorithm constraints were set so that for each raster scan position in the RBC interior the total hemoglobin concentration was 1 (i.e. $C[\mathrm{HbO_2}] + C[\mathrm{Hb}] = 1$), and further that $0 \leq C[\mathrm{Hb}], C[\mathrm{HbO_2}] \leq 1$.

III. Results and Discussion

A. Untreated RBCs

A fused RGB image of a representative untreated RBC is shown in Figure 2a, with the corresponding MMSE calculated SO_2 map in Figure 2b. A dark region in the center of the RBC can be seen in the fused image, as well as localized regions of high and low PA signal intensity around the cell periphery in both red and blue channels. The SNR in the image ranged from 8 in regions with low PA signal amplitude to 29 in regions with high PA signal. These fluctuations in signal amplitude may be due to differences in chromophore content throughout the RBC, or to interference between the forward traveling PA wave and PA waves reflected from the glass substrate. As previously discussed, many of these structural details are lost in the corresponding SO_2 map image, which only displays oxyhemoglobin concentration and neglects total hemoglobin content. The untreated RBC SO_2 map had a mottled appearance, with a majority of pixels having SO_2 greater than 60%. A histogram of SO_2 values for this image is shown in Figure 3a. The histogram distribution was skewed left, with a mean and median SO_2 value of 72 and 73%, respectively. This value is lower than the physiological arterial SO_2 value of approximately 97.5% [2]; however, this may be due to the effects of the glutaraldehyde fixation and/or the effect of gradual deoxygenation of the RBCs over time.

B. Treated RBCs

The bottom row of Figure 2 shows fused and SO_2 map images for a sodium dithionite treated RBC. Like the fused image of the untreated cell, the treated cell has a dark central region as well as patches of varying intensity at the cell periphery. Here however, regions of high signal in either the 560 nm image (coloured deep blue) or the 577 nm image (coloured bright red) can also be seen. These regions correlate with deoxygenated and oxygenated patches in the SO_2 map, respectively. As expected, there are significantly more pixels with low SO_2 in Figure 2d than in 2b, even though a ring of high SO_2 oxygenation is present at the edge of the cell. The SO_2 histogram for Figure 2d is shown in Figure 3b. Compared

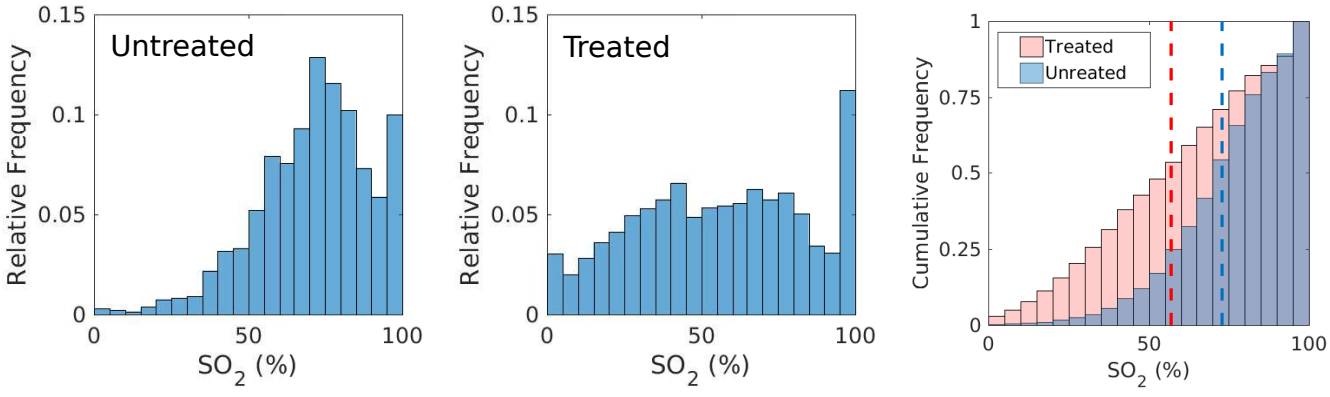

(a) (b) (c)

Fig. 3. Relative frequency histograms for the SO_2 of **a)** the untreated cell shown in Figure 2b, and **b)** the sodium dithionite treated cell shown in Figure 2d. **c)** Cumulative frequency histograms and median SO_2 value for the untreated cell shown in Figure 2b (blue), and the treated cell shown in Figure 2d (red).

to the skewed distribution of the untreated cell, the distribution in 3b is more uniform, with a mean and median value of 56 and 57% SO_2, respectively. The cumulative histograms in 3c accentuate the differences in the histogram data. The treated cell cumulative histogram is approximately linear with increasing SO_2, while the untreated cell cumulative histogram is sigmoidal in shape.

IV. Conclusion

High resolution SO_2 maps of untreated and sodium dithionite treated RBCs were created. The SO_2 map of the untreated cell showed a uniform distribution of high SO_2 values (> 60 %), while that of the treated cell had localized pockets of both high (> 60 %) and low (< 40 %) SO_2. The median SO_2 for the untreated and treated cells were 73% and 56%, respectively; demonstrating that the deoxygenating effect of sodium dithionite could be detected with the technique. Compared to other techniques that assess the SO_2 of individual RBCs, the presented technique has the advantage of high spatial resolution, but the disadvantage of slow image acquisition time at approximately 15 minutes per wavelength for a single RBC. In the future, additional SRS wavelengths will be used to improve the SO_2 value estimates, and different approaches for deoxygenating the RBCs will be explored.

Acknowledgment

This work was funded, in part, by the Natural Sciences and Engineering Research Council of Canada, the Canadian Cancer Society, the Canadian Foundation for Innovation, the Terry Fox New Frontiers Program Project, and the Ontario Ministry for Research and Innovation.

References

[1] F. Martini, M. Timmons, and R. Tallitsch, *Human Anatomy, 7ed.* Pearson Education, 2012.

[2] W. Beachey, *Respiratory Care Anatomy and Physiology: Foundations for Clinical Practice, 3ed.* Elsevier, 2013.

[3] K. K. Tremper and S. J. Barker, "Pulse Oximetry," *Anesthesiology*, vol. 70, pp. 98–108, 1989.

[4] J. A. Brunelle, A. M. Degtiarov, R. F. Moran, and L. A. Race, "Simultaneous measurement of total hemoglobin and its derivatives in blood using CO-oximeters: analytical principles; their application in selecting analytical wavelengths and reference methods; a comparison of the results of the choices made," *Scand J Clin Lab Invest*, vol. 56, no. S224, pp. 47–69, 1996.

[5] M. Ferrari and V. Quaresima, "A brief review on the history of human functional near-infrared spectroscopy (fNIRS) development and fields of application," *Neuroimage*, vol. 63, pp. 921–935, 2012.

[6] H. F. Zhang, K. Maslov, G. Stoica, and L. V. Wang, "Functional photoacoustic microscopy for high-resolution and noninvasive in vivo imaging," *Nat. Biotechnol.*, vol. 24, no. 7, pp. 848–851, 2006.

[7] X. Wang, X. Xie, G. Ku, L. V. Wang, and G. Stoica, "Noninvasive imaging of hemoglobin concentration and oxygenation in the rat brain using high-resolution photoacoustic tomography." *J. Biomed. Opt.*, vol. 11, no. 2, 2006.

[8] J. Yao, L. Wang, J.-M. Yang, K. I. Maslov, T. T. W. Wong, L. Li, C.-H. Huang, J. Zou, and L. V. Wang, "High-speed label-free functional photoacoustic microscopy of mouse brain in action." *Nat. Methods*, vol. 12, no. 5, pp. 407–410, 2015.

[9] L. Wang, K. Maslov, and L. V. Wang, "Single-cell label-free photoacoustic flowoxigraphy in vivo," *Proc. Natl. Acad. Sci. U. S. A.*, vol. 110, no. 15, pp. 5759–5764, 2013.

[10] J. Yao, K. I. Maslov, Y. Zhang, Y. Xia, and L. V. Wang, "Label-free oxygen-metabolic photoacoustic microscopy in vivo." *J. Biomed. Opt.*, vol. 16, no. 7, p. 076003, 2011.

[11] S. Kim, Y.-S. Chen, G. P. Luke, and S. Y. Emelianov, "In vivo three-dimensional spectroscopic photoacoustic imaging for monitoring nanoparticle delivery," *Biomed. Opt. Express*, vol. 2, no. 9, pp. 2540–2550, 2011.

[12] A. Agrawal, *Nonlinear Fiber Optics, 5ed.* Academic Press, 2012.

[13] D. Koeplinger, M. Liu, and T. Buma, "Photoacoustic microscopy with a pulsed multi-color source based on stimulated Raman scattering," *IEEE Int. Ultrason. Symp. Proc.*, pp. 296–299, 2011.

[14] P. Hajireza, A. Forbrich, and R. Zemp, "In-vivo functional optical-resolution photoacoustic microscopy with stimulated Raman scattering fiber-laser source," *Biomed. Opt. Express*, vol. 5, no. 2, pp. 539–546, 2014.

[15] E. M. Strohm, M. J. Moore, and M. C. Kolios, "High resolution ultrasound and photoacoustic imaging of single cells," *Photoacoustics*, vol. 4, no. 1, pp. 36–42, 2016.

[16] E. M. Strohm, M. J. Moore, and M. Kolios, "Acoustic and photoacoustic microscopy of single leukocytes," *Proc. SPIE*, vol. 9708, pp. 97 082G1–5, 2016.

[17] J. T. Coin and J. S. Olson, "The rate of oxygen uptake by human red blood cells," *J. Biol. Chem.*, vol. 254, no. 4, pp. 1178–1190, 1979.